



## Map portfolio of *Octopus vulgaris* off Mauritania

Dedah Ahmed-Babou, Hervé Demarcq, Beyah Meissa, Nicolas Bez

### ► To cite this version:

Dedah Ahmed-Babou, Hervé Demarcq, Beyah Meissa, Nicolas Bez. Map portfolio of *Octopus vulgaris* off Mauritania. 2022. hal-03649730v1

**HAL Id: hal-03649730**

**<https://hal.science/hal-03649730v1>**

Preprint submitted on 22 Apr 2022 (v1), last revised 10 Apr 2023 (v2)

**HAL** is a multi-disciplinary open access archive for the deposit and dissemination of scientific research documents, whether they are published or not. The documents may come from teaching and research institutions in France or abroad, or from public or private research centers.

L'archive ouverte pluridisciplinaire **HAL**, est destinée au dépôt et à la diffusion de documents scientifiques de niveau recherche, publiés ou non, émanant des établissements d'enseignement et de recherche français ou étrangers, des laboratoires publics ou privés.

# Map portfolio of *Octopus vulgaris* off Mauritania

Dedah AHMED-BABOU<sup>(1,2,3)</sup>, Hervé DEMARCQ<sup>(3)</sup>, Beyah MEISSA<sup>(1)</sup>, Nicolas BEZ<sup>(3)</sup>

1. IMROP, Nouadhibou, Mauritania
2. Ministry of Fisheries and Maritime Economy, Nouakchott, Mauritania.
3. MARBEC, IRD, Univ Montpellier, Ifremer, CNRS, INRAE, Sète, France

**Aim:** This study aims to identify the octopus's main recurrent spatial patterns, a cornerstone stock of the Mauritanian ecosystem, during each spawning season. Furthermore, it coins the map portfolio concept and shows how it can be developed in real case studies.

**Location:** Mauritania

**Taxon:** *Octopus vulgaris*

**Methods:** The principal spatial maps are a subset of the empirical orthogonal maps of the full dataset. Maps are first selected so as to recover 60% of the input variability. Amongst them, maps whose amplitude through time were significantly correlated with abundance are subselected.

**Results:** During the hot season, one single principal map explains half (48%) of the overall variability of the initial data. Its amplitude is strongly correlated with the abundance of octopus. During the cold season, the biogeography of octopus is more composite. Ten spatial patterns are needed to explain 62% of the initial variability. Five of these are correlated with abundance and have strong spatial structures. One map shows a significant correlation with the upwelling index six months before and represents the part of the spatial patterns connected with this key environmental factor.

**Main conclusions:** Based on octopus case study, the concept of a map portfolio is put forward. In the present case, its size represents the number of spatial patterns from which the octopus mainly composed its distribution over the past three decades. Assuming that specific but hidden processes explain each biomass distributions of the portfolio, its size could be a proxy for the systems' resilience. For a large portfolio, a process could decrease without damaging the overall system if compensated by an other process. Small portfolio could be symptomatic of more fragile systems. One perspective of this work could be to quantify the sizes of many portfolios and connect them to knowledge about the resilience of the system they characterize.

## Introduction

In ecology, monitoring and information systems are more and more numerous worldwide. They are key to providing long-term and sometimes very long-term observations. They contribute to drawing perspective, which is particularly important when dealing with reference points, tipping points, or regime shifts. Aside from their maintenance, one of the main challenges associated with the monitoring system is making the best out of them in terms of scientific knowledge. A recurrent challenge, for instance, is to evaluate whether we can define the main spatial patterns that emerge from large sets of georeferenced observations; and, if so, to evaluate how stable or variable these main spatial patterns are through time.

In marine ecosystems, numerous case studies exist with standardized and constant protocols in the long run (the list of regular scientific surveys performed on a routine base is quite long, and giving references would be either too long or restrictive). Amongst all, the ideas developed in this paper are illustrated in a specific case study devoted to octopus (*Octopus vulgaris*) off Mauritania over the past thirty years. Octopus represents a key species of the marine ecosystem both in ecological and economic terms, which fluctuates over large spatial and temporal scales (Boyle & Boletzky, 1996; Caddy, 1983). This variability in abundance is mainly a consequence of fluctuations in recruitment that are partly dependent on environmental conditions, especially the intensity of upwelling (Caverivière et al., 1999; Otero et al., 2008) and of the existence of two spawning periods that take place under distinct environmental conditions (Faure et al., 2008).

Since 1982, a dedicated monitoring system has been developed to feed the scientific process of providing advice to octopus management bodies (Gascuel et al., 2007). At its heart, the Mauritanian scientific community has performed a large time series of scientific surveys providing information on octopus spatial distributions through time, of which recurrent spatial patterns and/or tipping points of change in spatial distribution would be important to track. Revealing the mechanisms that shape the spatial distribution of the *Octopus vulgaris* through time requires that we can identify if they exist, some spatial patterns that best characterize the spatial distribution of the Octopus.

This study aims to develop a generic framework for simplifying the overall spatio-temporal information contained in a substantial time series of spatial distributions into a product of two simple and independent signals, one time-dependent and the other, possibly low-dimensional, space-dependent. This framework is based on empirical orthogonal functions (EOFs) (Lorenz, 1956). The number of output factors is often reduced to a few key factors that are represented as spatial distributions. However, EOFs are not, per se, spatial. The results are not sensitive to the geographic location of the input data. The min-max autocorrelation factor (MAF) (Switzer & Green, 1984) can be seen as an extension of EOFs to deal with the presence of spatial structure in the data and has led to some relevant applications in ecology (Petitgas et al., 2020; Solow, 1994; Woillez et al., 2009). However, MAF was initially designed to filter out small-scale noise from a set of images. So the percentage of variance explained by the selected factors is unknown.

In a recent paper, (Bez et al., 2022) suggested that MAF could be appropriately reformulated into Empirical Orthogonal Maps (EOMs) that order the factors according to the percentage of variance they explained. Therefore, the initial set of distribution maps can be reduced to a small number of principal orthogonal maps, primarily losing as less as possible information and, secondly, promoting as much as possible maps having the strongest spatial autocorrelation. The present work first defines how the empirical orthogonal maps are formulated and selected, and then indicates a possible way to analyze their mutual temporal variations. Based on this well-established methodology, we characterize the biogeography of octopus in Mauritanian waters by exhibiting empirical orthogonal maps of a large time series of sixty-one different scientific surveys over the period 1987- 2017. In conclusion, we address the possibility of formalizing the map portfolio concept. In particular, the size of the map portfolio, i.e., the number of principal spatial distributions needed to summarize each spawning season, is presented as an interesting concept to explore further.

## **Materials and methods**

### **Scientific monitoring surveys**

Between 1987 and 2018, the Mauritanian Institute of Oceanographic Research and Fisheries (IMROP) performed sixty-one scientific bottom trawl demersal surveys over its continental shelf (Figure 1a). The sampling protocol was standardized over the entire period and followed a stratified random protocol based on three latitudinal strata (Figure 1). The target was to record between 100 and 120 samples per survey, equally distributed over strata. The observations consisted of the octopus density expressed in the number of individuals per square meter obtained by dividing the catches by the surface of the area swept by the trawl. These were considered an indicator of abundance under the assumption that the catchability of the gear remains constant. More details on these data are available in (Gascuel et al., 2007), (Meissa et al., 2013), (Meissa & Gascuel, 2015).

For each survey, the positions of the stations were randomly selected and mutually independent. The observations were thus not collected at the same points every time (full heterotopy; (Wackernagel, 2003)). Data were kriged on a  $0.1^\circ \times 0.1^\circ$  grid covering the sampling area before analysis to generate isotopy. A block kriging was performed to estimate the mean octopus density by grid cell. The input data of the analyses were thus the sixty-one kriging maps.

Upwelling strength over the same period was built from a monthly dataset of the meridian component (North-South) of composite wind speeds over the Mauritanian zone, 50 to 100 km from the coast. This proxy was considered the best proxy linearly linked to the upwelling index for a North-South oriented coast (Demarcq & Faure, 2000), which is the case for the study area.

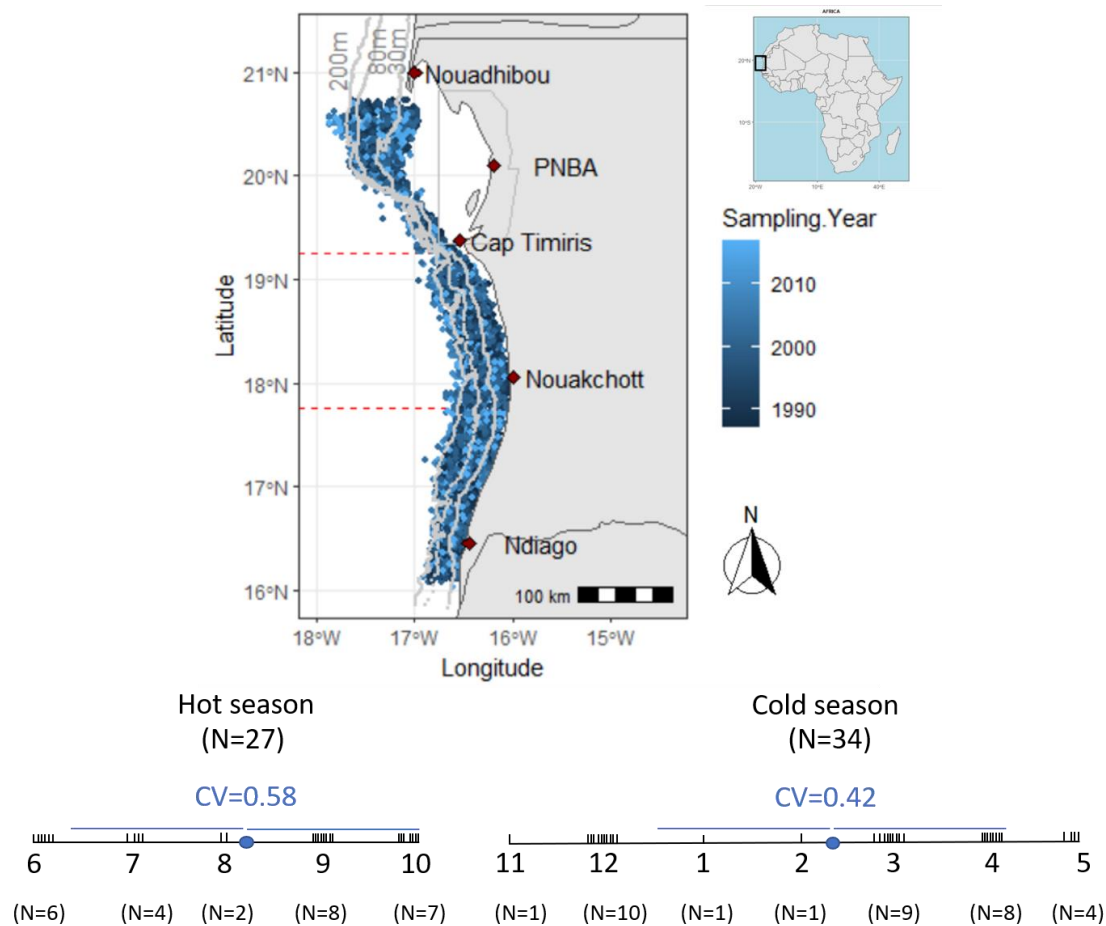


Figure 1 (a) Spatial distribution of sampling stations during the study period. PNBA = Parc National du Banc d'Arguin. The three latitudinal strata (North, 20°36'N-19°15'N; Central, 19°15'N-17°45'N; and South, 17°45'N-16°03'N) are represented by dashed lines. (b) Timing of the surveys for each of the hot and the cold seasons. The mean and the coefficient of variation of the timing by season are given in blue.

Four unequal climatic seasons are generally distinguished in the Mauritanian zone (Dobrovine et al., 1991). A cold season from January to May, a cold-warm transition season from June to July, a hot season from August to October and a hot-cold transition season from November to December. These four seasons were aggregated into two main seasons of five and seven months respectively: the hot season from June to October including 27 of the 61 available surveys, and the cold season for the rest of the year (November-December and January-May) including the remaining 34 surveys (Figure 1b). The precise timing of the surveys within each season was opportunist rather than following a predefined sampling protocol. This led to irregular spreading of the surveys which was of the same level in each season (same coefficients of variation; Figure 1b).

## Empirical orthogonal maps

The concept of empirical orthogonal maps (Bez et al., 2022), see graphical abstract (Figure 2), was recently coined as a declination of the Min-max autocorrelation factor (Switzer & Green, 1984) where the factors are ordered according to their contribution to the input variance. The first EOM corresponds to the principal map explaining most of the input variance, and so on down to the last EOM. This approach also attributes coordinates to each observed spatial distribution into an orthogonal space whose axes correspond to EOMs.

## Building EOMs

Notations used in this study allow switching between matrix writing (upper case) used in the supporting information (see Appendix), and spatio-temporal writing (lower case) that makes the spatio-temporal factorization more explicit. We denote  $x_i, i = 1, \dots, S$  the geographical positions of the  $S$  grid nodes that were systematically informed (isotopy) at time  $t_j, j = 1, \dots, T, T$  being the number of input maps ( $S = 533, T = 61$ ). The matrix of all observations is an  $S \times T$  matrix denoted  $Z[i, j] = z(x_i, t_j)$ . The rows  $z_i = Z[i, \cdot]$  are vectors with size  $T$  (called  $T$ -vectors) corresponding to the observations at a given position  $x_i$  over time. The columns  $z_j = Z[\cdot, j]$  are  $S$ -vectors corresponding to the observations for the input map that took place at time  $t_j$ . Computing EOMs consists of two sequential PCAs. The first PCA, which is nothing but an EOF, produces an  $S \times T$  matrix, denoted  $Y$ , with  $T$  uncorrelated variables usually called factors,  $y_j = y(\cdot, t_j)$ :

$$\rho_{y_j, y_{j'}}(0) = \langle y_j, y_{j'} \rangle = \sum_{i=1}^S y(x_i, t_j) y(x_i, t_{j'}) = 0 \quad \forall j \neq j'$$

In the spatio-temporal context, each factor is a set of georeferenced point, i.e. a map, that is uncorrelated to the others. The absence of correlation between factors refers to pointwise correlation, therefore, to the absence of correlation between factors' values at the same geographical points. However, these factors may exhibit spatial correlations because the covariance between columns of  $Y$  for different points (i.e. rows) may not be zero. The second PCA aims at building  $T$  new factors  $\psi_j = \psi(\cdot, t_j)$  without mutual spatial correlation for a given spatial distance  $\sigma$  (a trivial spatial lag corresponds to the pixel size of the input maps), that is with the following null scalar products:

$$\rho_{\psi_j, \psi_{j'}}(\sigma) = \sum_{i=1}^S [\psi_j(x_i), \psi_{j'}(x_i + \sigma)] = 0 \quad \forall j \neq j'$$

Finally, we obtain a set of new maps called empirical orthogonal maps – EOMs which are mutually uncorrelated for distance 0 and distance  $\sigma$ . Assuming that they are also orthogonal for all distances, allowed considering that they are fully spatially orthogonal. This leads to the following factorization of the initial spatio-temporal variables  $z(x_i, t_j)$  into a product of

two components, one component made of a set of spatially uncorrelated maps denoted  $\psi_k(x_i)$ , and the other component made of their temporal scores or amplitudes  $c_k(t_j)$ .

$$z(x_i, t_j) = m(t_j) + \sum_{k=1}^T c_k(t_j) \times \psi_k(x_i)$$

where  $m(t_j)$  is the average of each input map. At this stage, the decomposition is performed without losing any information. The two writings are fully equivalent. EOMs can be computed for raw or standardized map sets in their full genericity. The pseudo-algorithm provided in the supplementary material highlights the main steps in computing EOMs when the first PCA is applied to standardized ones.

The signs of the values of the EOMs and their scores are conventional. Therefore, their interpretation must be established jointly. For example, the interpretation of an EOM whose scores are all negative in the decomposition is strictly equivalent its symmetry with respect to 0 when taking the symmetry of both the EOM and its scores. Therefore, the EOM values must be interpreted in conjunction with their scores.

### **Selection of the most relevant EOMs**

Being a PCA type of approach, one can reduce the number of principal maps down to a small enough number to capture a significant part of the variability of the original maps without losing too much of the input information. The approximation of the input maps by the first  $Q$  EOMs writes:

$$\hat{z}(x_i, t_j) = m(t_j) + \sum_{k=1}^Q c_k(t_j) \psi_k(x_i)$$

The selection of the EOMs kept for the analysis was based on the following three embedded criteria: the percentage of variability they explained, with a target of explaining at least 60% of the input variability, the strength of their spatial structure, with a target to get small percentage of nugget effect and, the statistical significance of their linear relationship with abundance (p-value of the linear regression slope between abundance and their coefficients smaller than 5%).

### **Temporal joint dynamic of the principal distributions**

When several principal spatial patterns were selected, their temporal joint dynamic was investigated through simple and cross-variograms (Chilès & Delfiner, 2012) of the EOMs' temporal scores. To facilitate the interpretations, the cross-variograms were scaled to cross-correlations. A linear model of coregionalization (Wackernagel, 2003) was inferred according to (Goulard & Voltz, 1992) and was used to diagnose the mutual temporal dependencies between time series of EOM's scores. Temporal cross correlations with abundance wer also investigated.

## Climatology

When several principal spatial patterns were selected, a climatological spatial pattern was also computed by an average of the selected EOMs weighted by their average coefficients:

$$\bar{z}_Q(x_i) = \bar{m} + \frac{\sum_{k=1}^Q \bar{c}_k \times \psi_k(x_i)}{\sum_{k=1}^Q \bar{c}_k}$$

where  $\bar{c}_k$  is the mean amplitude of a given selected EOM over time:

$$\bar{c}_k = \frac{1}{T} \sum_{i=1}^T c_k(t_j), \quad k = 1, \dots, Q$$

and where  $\bar{m}$  is the mean abundance over time:

$$\bar{m} = \frac{1}{T} \sum_{i=1}^T m(t_j)$$

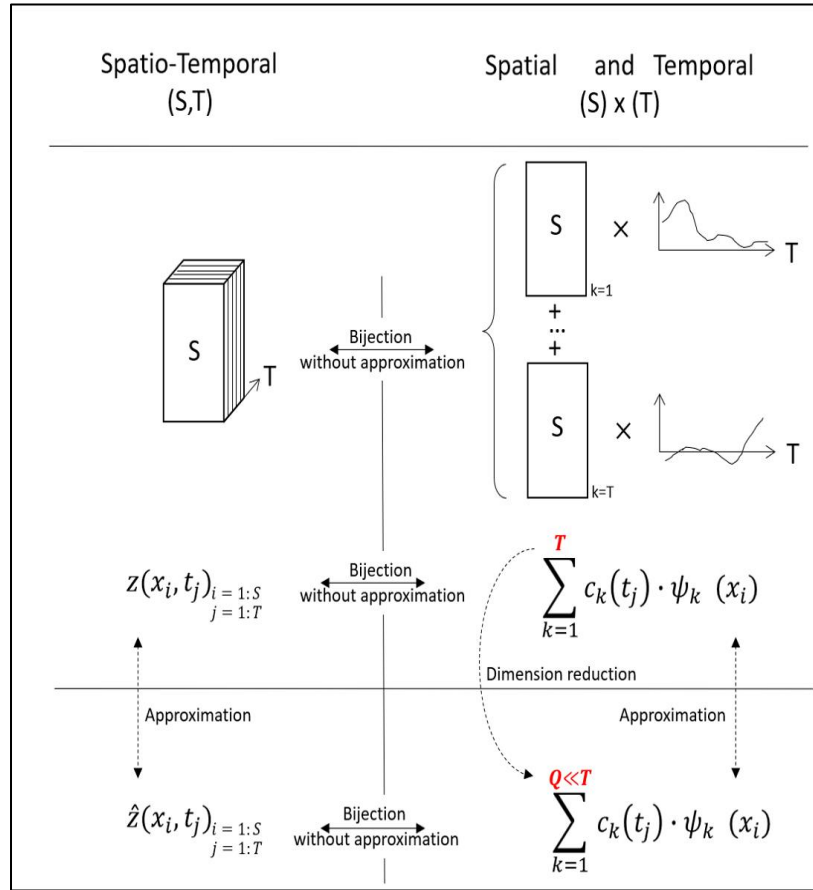
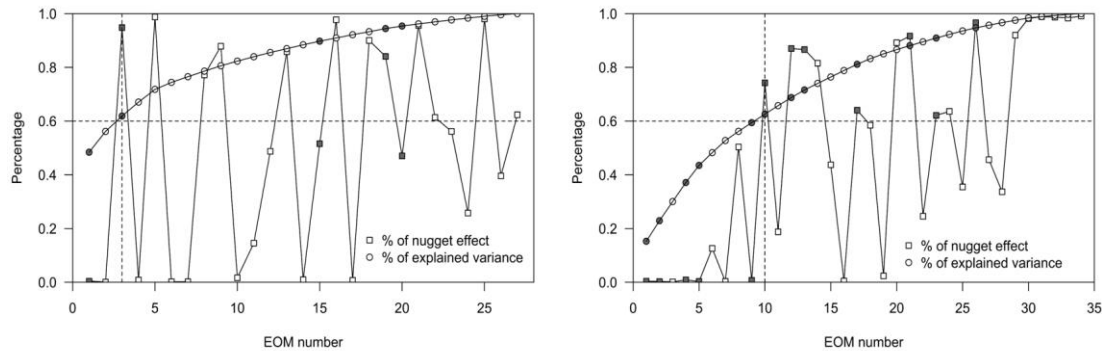


Figure 2. Graphical abstract of the method.



## Results

In the Mauritanian zone, the existence of two annual cohorts of octopus with two distinct spawning seasons ((Hatanaka, 1979); (Bez et al., 2022)) justifies the implementation, separately, of this approach for each of the two seasons.



*Figure 3. Descriptive statistics of the EOM. Percentage of variance explained by increasing nested sets of EOMs and percentage of nugget effect in the EOM spatial structure. Hot season (left) and cold season (right). Black features correspond to EOMs whose coefficients are significantly correlated to abundance over time ( $p$ -value  $< 0.05$ ).*

### Maps portfolio of the hot season

The main octopus breeding season is during the hot season in Mauritanian waters (from June to October). The results indicate that the first EOM alone restores 48% of the variability of the observed data (Figure 3), and the first three recover 60% of the initial variability and have well defined spatial structures without local heterogeneity (no nugget effect). The scores of the first principal map (EOM1) show a strong correlation with the abundance (correlation = 0.79;  $p$ -value =  $7.4e-07$ ; Figure 4) while the second (EOM2) does not show significant linear relationships. Although the third shows a significant correlation with abundance, it is not spatially structured. Thus, the hot season portfolio was only made of the first principal map. It is characterized by a north-south gradient, with a rich area in the north (especially in its wide part), a moderately rich area in the center and a poor area in the south (Figure 4). The temporal evolution of the scores of the first principal map shows three different phases. There is a sharp decrease over the first five years followed by a flat behavior and a positive recovering trend over the past twenty years.

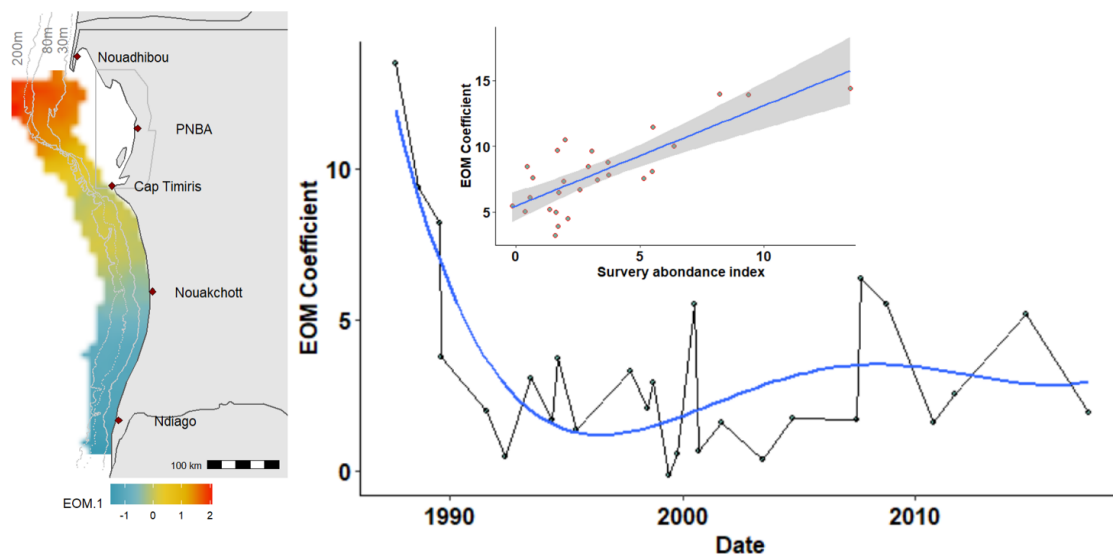


Figure 4. First EOM (left), and the temporal evolution of its coefficients smoothed by a polynomial of degree 4. The correlation plot (top right) crosses mean abundance and EOMs' scores.

## Maps portfolio of the cold season

The results indicate that the spatio-temporal complexity is more pronounced during the cold season than during the hot season (Figure 3). No spatial pattern was predominant on its own. Indeed, the first EOM explains only 18% of the variability of the input spatial data and the first ten EOMs restore 62% of the variability. Five of these top ten EOMs, respectively the 1st, 2nd, 4th, 5th and 9<sup>th</sup>, show significant correlations with the observed mean abundance, however with a different order ( $\rho_{2,Ab} = 0.76 > \rho_{4,Ab} = 0.62 > \rho_{5,Ab} = 0.58 > \rho_{1,Ab} = 0.49$  and  $\rho_{9,Ab} = 0.55$  for the EOM9 that was put aside for reasons explained below).

The spatial pattern of the first EOM is similar to that of the hot season, characterized by an overall north / south gradient with a slightly different temporal evolution. The 2nd EOM represents a rich area south of Nouakchott, offshore, and a poor area in the extreme south. The 4th EOM highlights two rich zones, the north and the central zones, that correspond to the main zones of the presence of the population in general (Faure et al., 2008). This spatial pattern reinforces, to the north, the spatial pattern of the first EOM1, but complements it in the central zone. The last two EOMs correlated with abundance, namely the 5th and the 9th, display across-shelf gradient patterns, opposing poor coastal areas to rich offshore areas.

The selected EOMs have similar long term temporal variations of their scores (Figure 5). They decrease at the beginning of the period, then flatten and slightly increase during 2010-2015. At short temporal scales, in the late 90s, a substitution effect is noticeable between EOM 1 and 2 whose scores show opposite values regarding the trend (EOM 2 grows while EOM 1 diminishes).

The climatological spatial pattern associated with the cold season is characterized by two rich areas rather offshore (Figure 5, Right). A northern zone off Cape Blanc whose epicenter is located between the bathymetric lines of 80 and 200m. A second zone, south of the Cap Timiris (in the middle of the central zone), with an extension to a bathymetric level close to that of the northern zone.

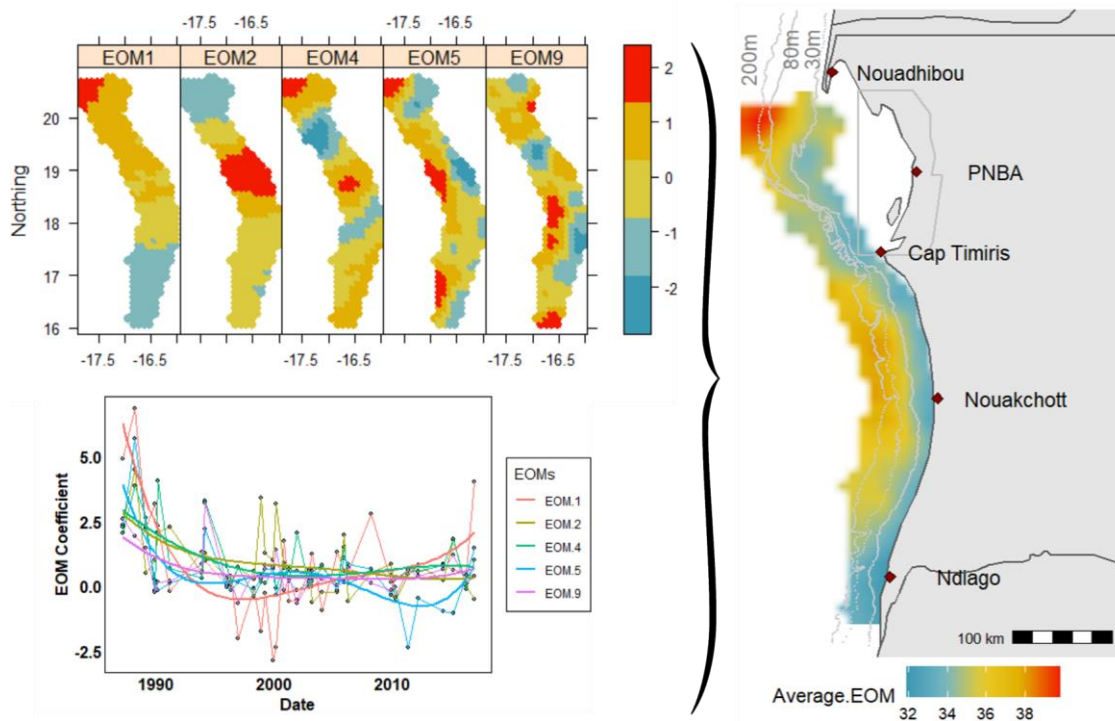


Figure 5. Left: principal maps (maps' portfolio) of the cold season and their temporal evolution. A smoothing by a polynomial of degree 4 is superimposed (solid lines). Right: average spatial patterns of the cold season (climatology).

The scores of the selected EOMs are not statistically different for surveys carried out in December and in March or April (Figure 6), except for EOM9 whose scores are larger in March-April than in December (Student p-value = 0.008).

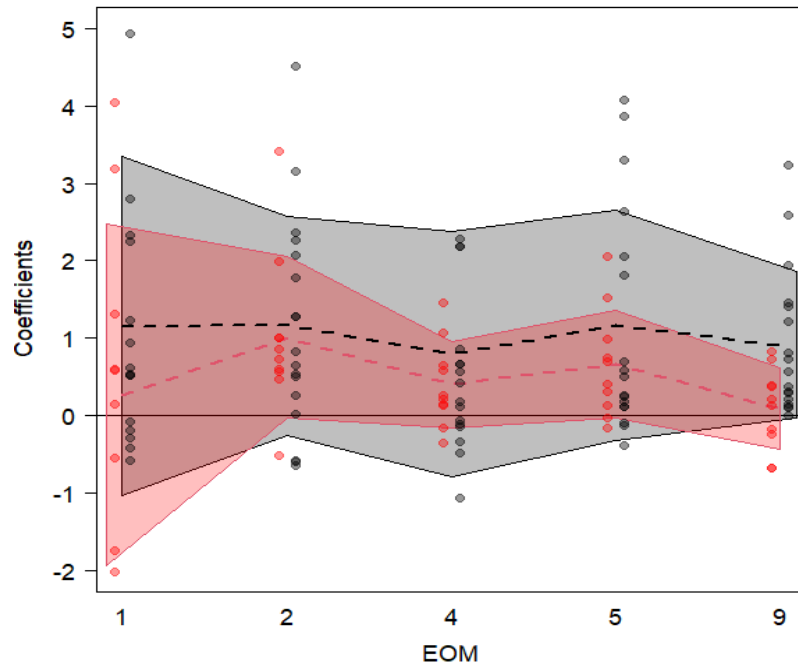


Figure 6. Distribution of the EOMs' scores as a function of the timing of the input surveys. The scores for the surveys carried out in March and April ( $N=17$ ) are represented in black. The scores for surveys performed in December ( $N=10$ ) are given in red. The polygons delineate the average  $\pm$  the standard deviations.

The joint temporal variations of the EOMs' scores and abundance was explored by analyzing their temporal simple and cross-correlograms. One EOM, namely EOM9, shows clear periodic variations of 6 years (Figure 7a). Its analysis is summarized to the next section dedicated to correlation with the upwelling intensity. The four other scores time series are composed of two temporal processes with contrasting temporal scales: a pure noise called the nugget effect (intercept) and long term linear trends (Figure 8, diagonal panels). It can be noticed that the two processes are well balanced except for EOM2 for which the part of the pure random noise is predominant (72%). The intercept corresponds to the part of the spatial pattern that varies from year to year without any memory. The linear part corresponds to long-term memory similar to that of a random walks process.

The cross-correlograms (Figure 8, lower triangle black boxes) indicate no nugget effects (except the cross-correlogram between EOM1 and 2 which shows small negative short-term temporal correlation). This result indicates that temporal variations of the principal maps are correlated in the long term but that their year-to-year fluctuations are independent.

The analysis of the temporal cross-correlograms between the EOMs' scores and the abundance shows that the fluctuations of the temporal correlations are due to the nugget effect only (Figure 8, lower triangle red boxes). In other words, EOM2 is more correlated over time to abundance than EOM1 because the year-to-year fluctuations of EOM2 are more correlated with abundance than those of EOM1. However, the medium to long term parts of

the different signals are shared similarly (linear parts of the model). The cross-variogram between EOM2 and abundance is proportional to the simple variogram of abundance (but not to the variogram of EOM2). In geostatistical terms, this means that abundance is self-krigeable regarding EOM2 (Chilès & Delfiner, 2012). Thus, the residual from the regression of the EOM2's scores against abundance is a temporal white noise, i.e. a residual with no temporal auto-correlation (Figure 7). In practice, the reverse would have been more interesting, i.e. the possibility of inferring abundance from the score of the second principal map. However, this point is not supported by the observations.

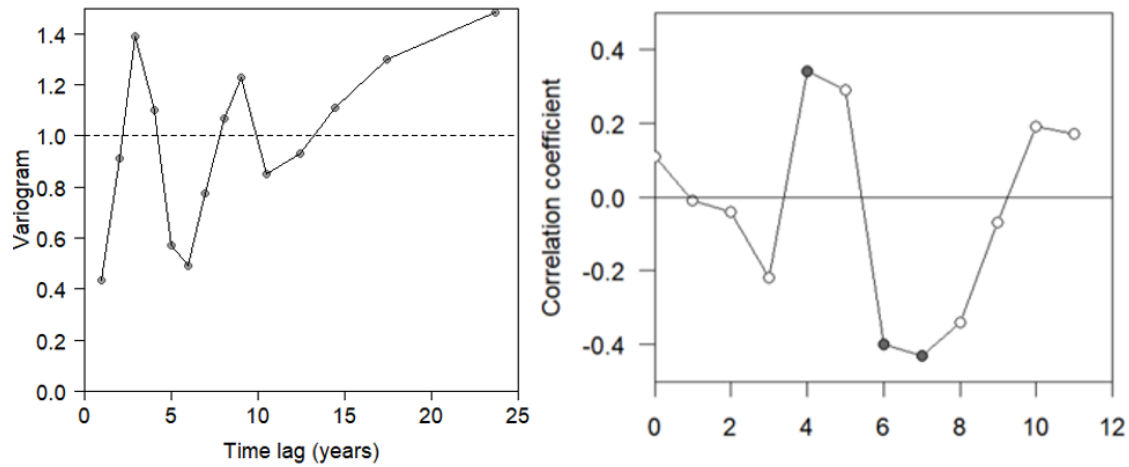


Figure 7. Analysis of the coefficients of EOM9 (cold season). Left: simple temporal variogram. Right: shifted correlation with upwelling index, one to eleven months before. Black rounds indicate shifts for which the correlation was significantly non-zero at the 5% level.

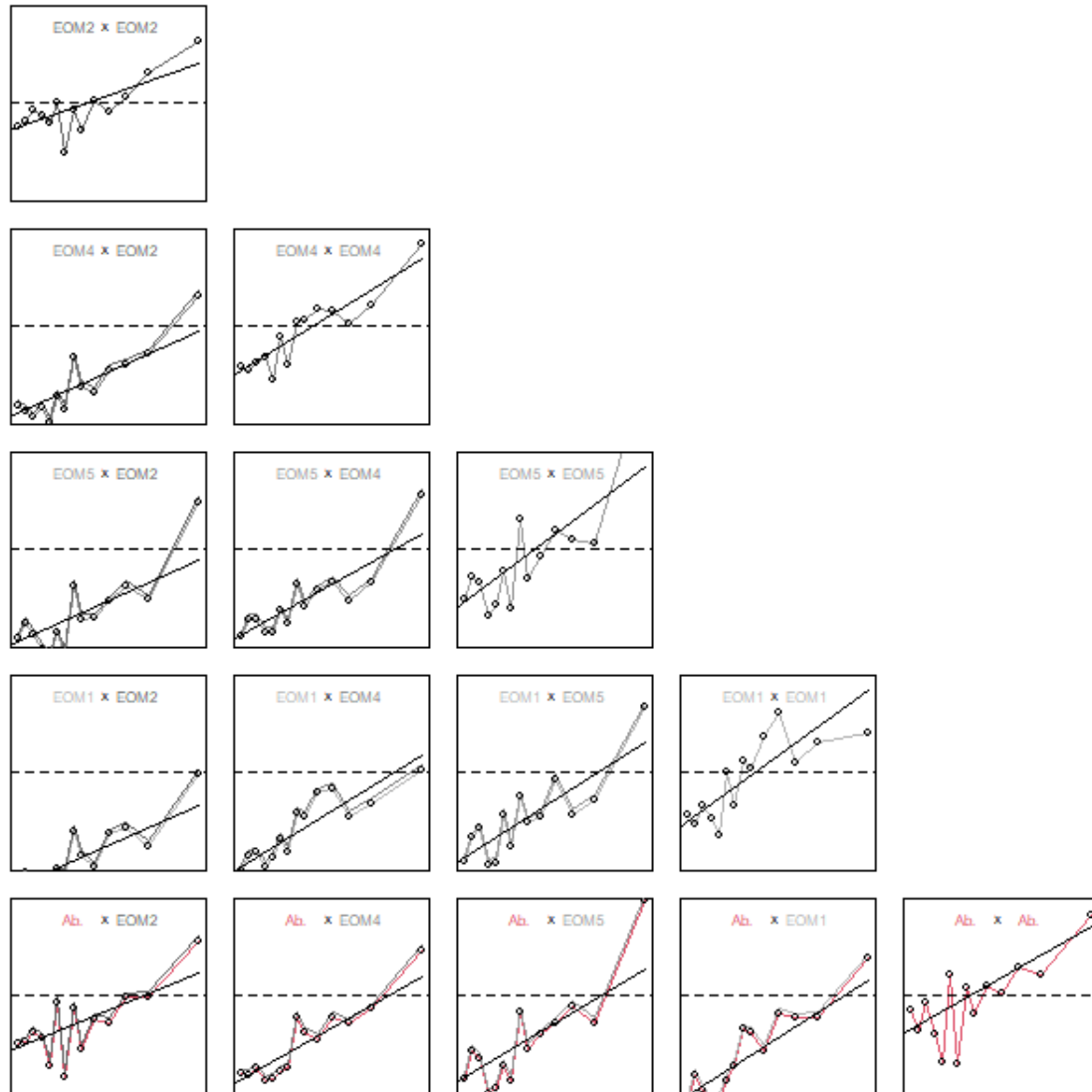
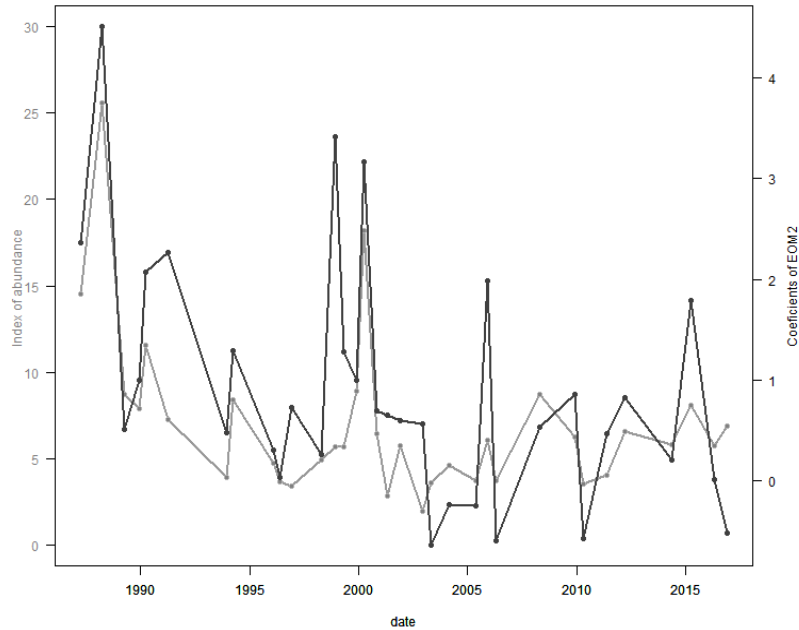


Figure 8. Analysis of the dynamic of the non-periodic principal spatial patterns (EOM 2, 4, 5, 1) for the cold season. EOMs are ordered by decreasing levels of correlation with abundance. The simple variograms are on the diagonal and the cross variograms on the lower triangles. Figures in black boxes correspond to the EOM between them. Figures in red boxes correspond to the analysis of the relationships with abundance. The linear model of coregionalization for the EOMs' coefficient and the abundance is superimposed on the empirical outputs.



*Figure 9. Time series of the abundance (grey) and the coefficient of the second EOM (black).*

## **Relationship between the pseudo-periodic EOM and coastal upwelling index**

EOM9's scores show an inter-annual periodic behavior and deserved analysis of its correlation with (a proxy of the monthly mean) upwelling indices in the area. This aim is to identify a possible link between the biogeography of the species described by EOM9 and the variability of some environmental conditions. While the octopus is a sedentary species during its adult phase, the para-larvae and planktonic phase, which lasts around three months, is likely influenced by the upwelling intensity. A delay in the correlation between the two was thus expected. It appears to be significantly different from 0 and negative, at the 5% null hypothesis threshold, with lags of 6 and 7 months (Figure 7 b).

## **Discussion**

The fact that the arrangement of principal maps in terms of the percentage of variance they explained (EOM) strongly matches the arrangement based on the strength of their spatial structures (MAF) is worth mentioning. It may be that the most important principal maps are the maps without spatial structure, with hot spots appearing here and there from survey to survey. In this study, spatial patterns are recurrent, and looking for climatologies was an appropriate step.

In an ideal situation, one would obtain a regular spread of the scientific surveys over time. This was not the case in the present study. For instance, during the cold season, surveys took place mainly in December (N=10) or in March (N=9) and April (N=8). However, the EOMs are not associated with specific months or a couple of months. For instance, EOM5 is not dominant for restoring distribution maps observed in March and April, while EOM4 can explain those of December. Therefore, the five EOMs selected for the cold season (November-May) were considered, as a whole, as the set of principal spatial patterns that best summarized the octopus spatio-temporal distribution during that season. The analysis of the joint temporal dynamics of the different EOMs highlighted possible underlying processes explaining their mutual correlations. In particular, EOM1, 2, 4, and 5 share the long-term trends while year-to-year variations are independent. In other words, during the cold season, the importances of the four principal maps fluctuate jointly and smoothly on the scale of several years, but not from year to year, where one could gain in importance while the others diminish.

The results indicate that the amplitude of EOM9 is periodic and significantly correlated to the upwelling activity six or seven months before. Meanwhile, the coefficients of EOM9 contributed significantly more to the March-April surveys than to those that took place in December. Thus, if we consider that EOM9 represents part of the spatial pattern that occurred in March-April, the six-seven-month delay in the correlation indicates upwelling conditions in August-September. Indeed, this is when it is at its minimum in terms of mixing energy and at its maximum in terms of water temperature (Arfi, 1987; Demarcq & Faure, 2000). The upwelling also demonstrates clear seasonal periodicities of six and twelve months. These different results suggest that the spatial pattern described by EOM9, with areas of high abundance offshore, occurred in spring when upwelling intensity is particularly low in late summer, i.e., when Ekman transport is low. This could be explained by a better settlement of octopus paralarvae that rise after spawning, which usually peaks earlier in summer (Balguerías et al., 2002).

The present study and the results suggest that a map portfolio's concept, particularly its size, can be of interest. During the hot season, the effective number of maps needed to summarize the set of observations is one, while it increases to five for the cold season. These two seasons achieved relatively identical temporal windows (five and seven months respectively) with a similar spread of survey dates within seasons. Thus, the difference in map portfolio size between the two seasons is not attributable to variations in the timing of the monitoring protocol. Instead, the difference in map portfolio size could be considered a consequence of a real difference in the spatial dynamics of octopus between the two seasons. The portfolio size quantifies the effective number of spatial patterns among which the octopus mainly composes its distribution. This was reduced to a single spatial pattern during the warm season in the present study. In contrast, the spatial distribution of octopus during the cold season was a mixture of five possible principal maps, one of which was related to the strength of the upwelling.

Ecological considerations arising from portfolio size can be of two kinds. Portfolio size measures the complexity and variability of spatial occupancy patterns and, the associated complexity and variability of possible external parameters governing them over time. On the one hand, large portfolio can characterize resilient systems: one process governing biomass



distribution can decrease without damaging the overall system if it is offset by other processes. On the other hand, systems associated with a small portfolio have less buffer effects and could be more fragile to external changes. Putting all the eggs in one basket is risky. Following these lines, a general perspective of this work could be to quantify the sizes of many portfolios and relate them to knowledge about the resilience of the system they characterize.

## Appendix

The following pseudo-algorithm highlights the main steps for calculating EOMs when the first PCA applies on standardised data (the meaning of the various superscript notations are the following:  $s$  means standardised,  $t$  means transposed and  $-1$  means inverse):

1. Subtract the mean of each input map. Mean abundances over the study area were estimated by averaging each kriging map and were expressed in numbers of individual per square meter. Build  $Z^s = ZD_s^{-1}$  their standardized version (centred and reduced) where  $D_s^{-1}$  is a  $T \times T$  diagonal matrix with the inverse of the standard deviation of the input maps on the diagonal. This step is often implicit in principal component analyses.
2. Calculate  $\rho$  the  $T \times T$  correlation matrix of  $Z$ , that is the variance matrix of  $Z^s$ .
3. Diagonalize  $\rho = VD_\lambda V^t$  to obtain the diagonal matrix  $D_\lambda$  of the eigenvalues and the matrix  $V$  of the corresponding eigenvectors.
4. Calculate  $Y = Z^s V$  the projection of  $Z^s$  in the space formed by the eigenvectors.
5. Reduce  $Y$  into  $Y^s = YD_{1/\sqrt{\lambda}} = Z^s V D_{1/\sqrt{\lambda}}$ .
6. Calculate the matrix  $\gamma_\sigma$  equals to twice the values of the simple and cross variograms of  $Y^s$  (for a chosen distance lag  $\sigma$ ).
7. Find the eigen-elements  $\lambda_\sigma$  and  $V_\sigma$  of  $\gamma_\sigma$  and rearrange them according to the variance explained in descending order (Bez et al., 2022). The rearrangement makes the difference between MAF (Switzer & Green, 1984) and EOM (Bez et al., 2022) decompositions.
8. Compute the EOM factors as  $\psi = Y^s V_\sigma = Z^s V D_{1/\sqrt{\sigma}} V_\sigma = Z^s P$  where  $P$  represents the linear operator that transforms the set of standardized input maps into a set of mutually uncorrelated standardized maps.
9. Calculate the temporal coefficients also referred to as amplitude of the decomposition  $C = P^{-1} D_s$ . Matrix  $C$  reads horizontally the time evolution of the importance of a given EOM, and matrix  $C$  reads vertically the linear combination of EOM required to recover a given input maps. In particular:  $C[k, j] = c_k(t_j)$ .

## Bibliography

- Arfi, R. (1987). Variabilité interannuelle de l'hydrologie d'une région d'upwelling (bouée Bayadère, Cap Blanc, Mauritanie). *Oceanologica acta*, 10(2), 151-159.
- Balguerías, E., Hernández-González, C., & Perales-Raya, C. (2002). On the identity of *Octopus vulgaris* Cuvier, 1797 stocks in the Saharan Bank (Northwest Africa) and their spatio-temporal variations in abundance in relation to some environmental factors. *Bulletin of Marine Science*, 71(1), 147-163.
- Baudrier, J., Lefebvre, A., Galgani, F., Saraux, C., & Doray, M. (2018). Optimising French fisheries surveys for marine strategy framework directive integrated ecosystem monitoring. *Marine Policy*, 94, 10-19. <https://doi.org/10.1016/j.marpol.2018.04.024>
- Bez, N., Renard, D., & Ahmed-Babou, D. (2022). *Empirical Orthogonal Maps (EOM) and distance between empirical spatial distributions. Application to Mauritanian octopus distribution over the period 1987-2017*. <https://hal.archives-ouvertes.fr/hal-03338408>
- Blangiardo, M., Cameletti, M., Baio, G., & Rue, H. (2013). Spatial and spatio-temporal models with R-INLA. *Spatial and Spatio-Temporal Epidemiology*, 4, 33-49. <https://doi.org/10.1016/j.sste.2012.12.001>
- Boyle, P. R. (1996). Cephalopod populations : Definition and dynamics. *Philosophical Transactions of the Royal Society of London*, 351(1343), 985-1002.
- Caddy, J. F. (1983). The cephalopods : Factors relevant to their population dynamics and to the assessment and management of stocks. *Advances in assessment of world cephalopod resources*, 231, 416-449.
- Caverivière, A., Domain, F., & Diallo, A. (1999). Observations on the influence of temperature on the length of embryonic development in *Octopus vulgaris* (Senegal). *Aquatic Living Resources*, 12(2), 151-154.
- Chiles, J. P., & Delfiner, P. (2009). *Geostatistics : Modeling Spatial Uncertainty* (Vol. 497). John Wiley & Sons.
- Demarcq, H., & Faure, V. (2000). Coastal upwelling and associated retention indices derived from satellite SST. Application to *Octopus vulgaris* recruitment. *Oceanologica Acta*, 23(4), 391-408. [https://doi.org/10.1016/S0399-1784\(00\)01113-0](https://doi.org/10.1016/S0399-1784(00)01113-0)
- Diallo, M., Jouffre, D., Caverivière, A., & Thiam, M. (2002). The demographic explosion of *Octopus vulgaris* in Senegal during the summer 1999. *Bulletin of marine science*, 71(2), 1063-1065.

- Dobrovine, B., Ould Mohamed Mahfoud, M., & Ould Sidina, D. (1991). *La ZEE mauritanienne et son environnement géographique géomorphologique et hydroclimatique*. Bulletin Scientifique du CNROP. <https://aquadocs.org/handle/1834/518>
- Faure, V., Inejih, C., Demarcq, H., & Cury, P. (2008). The importance of retention processes in upwelling areas for recruitment of *Octopus vulgaris* : The example of the Arguin Bank (Mauritania). *Fisheries Oceanography*, 9, 343-355. <https://doi.org/10.1046/j.1365-2419.2000.00149.x>
- Gascuel, D., Labrosse, P., Meissa, B., Taleb Sidi, M. O., & Guénette, S. (2007). Decline of demersal resources in North-West Africa : An analysis of Mauritanian trawl-survey data over the past 25 years. *African Journal of Marine Science*, 29(3), 331-345.
- Girardin, M. (1990). Evaluation par chalutage des stocks démersaux du plateau continental mauritanien en 1987 et 1988. *Bulletin Scientifique du CNROP*, 21. <http://hdl.handle.net/1834/807>
- Goulard, M., & Voltz, M. (1992). Linear coregionalization model : Tools for estimation and choice of cross-variogram matrix. *Mathematical Geology*, 24(3), 269-286.
- Hatanaka, H. (1979). Studies on the fisheries biology of common octopus off the northwest coast of Africa. *Bull. Far Seas Fish. Res. Lab.*, 17, 13-124.
- Katsanevakis, S., & Verriopoulos, G. (2006). Seasonal population dynamics of *Octopus vulgaris* in the eastern Mediterranean. *ICES Journal of Marine Science*, 63(1), 151-160. <https://doi.org/10.1016/j.icesjms.2005.07.004>
- Lindgren, F., Rue, H., & Lindström, J. (2011). An explicit link between Gaussian fields and Gaussian Markov random fields : The stochastic partial differential equation approach. *Journal of the Royal Statistical Society: Series B (Statistical Methodology)*, 73(4), 423-498. <https://doi.org/10.1111/j.1467-9868.2011.00777.x>
- Lorenz, E. N. (1956). *Empirical orthogonal functions and statistical weather prediction* (Vol. 1). Massachusetts Institute of Technology, Department of Meteorology Cambridge.
- Meissa, B., & Gascuel, D. (2015). Overfishing of marine resources : Some lessons from the assessment of demersal stocks off Mauritania. *ICES Journal of Marine Science*, 72(2), 414-427.
- Meissa, B., Gascuel, D., & Rivot, E. (2013). Assessing stocks in data-poor African fisheries : A case study on the white grouper *Epinephelus aeneus* of Mauritania. *African Journal of Marine Science*, 35(2), 253-267.

- Morfin, M., Fromentin, J.-M., Jadaud, A., & Bez, N. (2012). Spatio-Temporal Patterns of Key Exploited Marine Species in the Northwestern Mediterranean Sea. *PLoS ONE*, 7(5), e37907. <https://doi.org/10.1371/journal.pone.0037907>
- Otero, J., Álvarez-Salgado, X. A., González, Á. F., Miranda, A., Groom, S. B., Cabanas, J. M., Casas, G., Wheatley, B., & Guerra, Á. (2008). Bottom-up control of common octopus *Octopus vulgaris* in the Galician upwelling system, northeast Atlantic Ocean. *Marine Ecology Progress Series*, 362, 181-192.
- Petitgas, P., Renard, D., Desassis, N., Huret, M., Romagnan, J.-B., Doray, M., Woillez, M., & Rivoirard, J. (2020). Analysing Temporal Variability in Spatial Distributions Using Min–Max Autocorrelation Factors : Sardine Eggs in the Bay of Biscay. *Mathematical Geosciences*, 52(3), 337-354. <https://doi.org/10.1007/s11004-019-09845-1>
- RGeostats : The Geostatistical R Package. Version : 12.0.0. Free download from : [Http://rgeostats.free.fr/](http://rgeostats.free.fr/). (s. d.).*
- Semmens, J. M., Pecl, G. T., Villanueva, R., Jouffre, D., Sobrino, I., Wood, J. B., & Rigby, P. R. (2004). Understanding octopus growth : Patterns, variability and physiology. *Marine and Freshwater Research*, 55(4), 367-377.
- Solow, A. R. (1994). Detecting change in the composition of a multispecies community. *Biometrics*, 50(2), 556-565.
- Switzer, P., & Green, A. A. (1984). *Min/max autocorrelation factors for multivariate spatial imagery* (6) [Technical report].
- Thorson, J. T., Scheuerell, M. D., Shelton, A. O., See, K. E., Skaug, H. J., & Kristensen, K. (2015). Spatial factor analysis : A new tool for estimating joint species distributions and correlations in species range. *Methods in Ecology and Evolution*, 6(6), 627-637. <https://doi.org/10.1111/2041-210X.12359>
- Wackernagel, H. (2003). *Multivariate geostatistics* (Vol. 388). Springer Science & Business Media.
- Woillez, M., Rivoirard, J., & Petitgas, P. (2009). Using min/max autocorrelation factors of survey-based indicators to follow the evolution of fish stocks in time. *Aquatic living resources*, 22(2), 193-200.